COMPUTATION OF LOW SPEED FLOW PAST MULTI-ELEMENT AIRFOILS WITH LARGE FLOW SEPARATION*

Glen W. Zumwalt
Distinguished Professor
Department of Aeronautical Engineering
Wichita State University
Wichita, KS, U.S.A.

and

Rangasamy Elangovan
Senior Engineer
Boeing Military Airplane Company
Wichita, KS, U.S.A.

Abstract

Computation of flows around multi-element airfoils under landing and take-off conditions has great application. The problem is complicated by the presence of confluent boundary layers and large separated regions alongside lifting surfaces. Recent experimental data show that the reversed flow velocities in such separated regions are generally one-fourth to one-third that of the free stream. Thus, the mass and momentum in these wakes are too great to ignore.

The separated bubbles are treated separately with the velocity profiles predicted from jet mixing theory and semi-empirical shapes. The separation bubbles are termed "the inside flow"; this is matched iteratively with "the outside flow" at the bubble boundaries. The outside problem is treated by a potential flow method and a boundary layer computation, which gives the separation points. A new potential flow program was developed which can treat multiple elements of the airfoil and is of a combined direct-and-inverse type. This gives separated wake shapes for a specified pressure field. The "inside" solution provides pressure values in the iteration. There is a shortage of experimental data which is detailed enough to evaluate the computer program. However, flow field data (velocity and pressure) as well as surface pressures were available for a flapped GA(W)-1 airfoil, and this was used for computation test cases. The results correlated very well for either attached flow on the airfoil and well-separated flap, or vice versa. Surface pressures, force and moment coefficients and wake geometries were all used in comparisons.

The computation method is unique in its inclusion of the separation wake flows and pressures and its lack of pre-specification of the separation and recombination locations or pressures.

I. Introduction

Flaps are widely used on aircraft as high lift or drag devices. While in use, either the flap or the main wing is likely to have a large region of separated flow on its upper surface. There is need for a fast but accurate computational method for the flap with a gap (Fig. 1), since optimizing of the flap hinge point is a trial and error process. This search for the best hinge location at each flap deflection is generally done in a series of wind tunnel runs, with sizeable wind tunnel wall corrections needed due to the high lift coefficients. Further corrections are commonly required for scale-effects. If a computational method is economical and accurate, it may be preferred over experimental methods for design work.

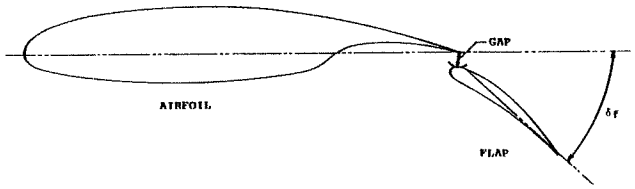

Figure 1. Airfoil with a Finite-Gap Flap.

The analytical method builds on three works done at Wichita State University in recent years. Naik and Zumwalt[1] used an inside-outside matching method for the separation wake bubble on a simple airfoil (Fig. 2). The outer flow portion considered the flow around an effective body formed by adding the closed wake to the airfoil geometry augmented by the boundary layer thickness. Flow around this effective body was solved by a potential flow program of the mixed-boundary condition type; either surface geometry or pressure could be specified. The inner flow problem described the flow within the closed wake. Mixing velocity profiles were developed and mass balances

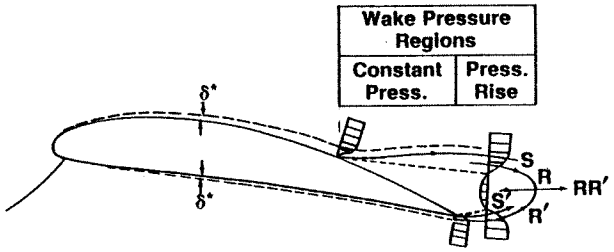

Figure 2. The Zumwalt-Naik Model.

*This paper is based on the Ph.D. dissertation of the second author at Wichita State University.

made resulting in an improved value of the pressure at the end of the wake (the "recompression region"). Separation location was allowed to change and iterations were made until convergence was reached. Experimental verification was good.

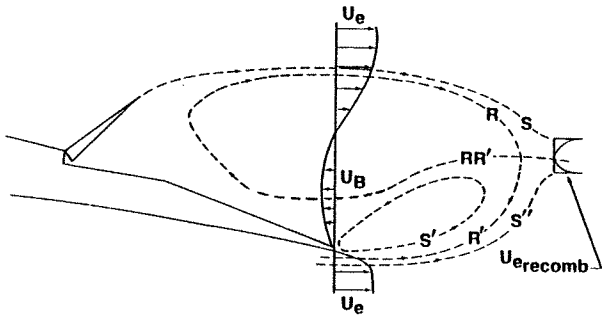

Figure 3. The Spoiler Wake Model.

An airfoil with a spoiler was treated by Pfeiffer and Zumwalt,[2] in an improved version of the inside-outside matching approach. Excellent agreement with experimental results was achieved for four different airfoils. Zumwalt and Carlson[3] adapted the method to airfoils with aileron-type airfoil control surfaces (Fig. 4). Both of these considered corner flow separation ahead of the control surface as well as the wake bubble behind it.

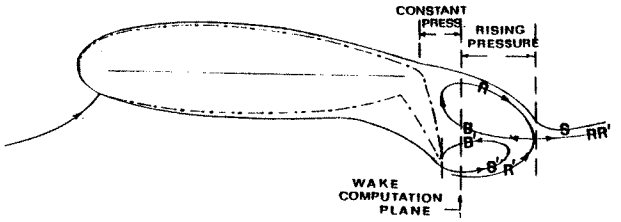

Figure 4. The Aileron Wake Model.

In all of these, the modeling philosophy was to include the principal physical features, namely, the back flow in the wake and the free stagnation point at the rear of the short, closed wake. Separation pressure and location were free to vary during the iterations and were determined in the computations. This project extended that philosophy to a multi-element airfoil while refining several of the elements of the previous works. In particular, a completely near potential program similar to the single element program of Maskew[4] was developed with multi-element and mixed-boundary-condition capability and more efficient computational elements. Incompressible, steady flow was assumed. Details and computer program listings are given in References 5 or 6.

II. Flow Description

It was considered axiomatic that analytical modeling should be preceded by careful observation of the physics of the flow field. In a parallel experimental study under Prof. W.H. Wentz at Wichita State University, detailed flow field, surface pressures, force and moment measurements were made for the GA(W)-1 airfoil with an optimized 30% flap. Figures 5 and 6 are typical flow fields.[7] In Figure 6, the flow is seen to be separated for over half of the flap upper surface. Figure 5 shows the short length of the reversed flow wake. Pressure field surveys have established that pressure in the wake is essentially constant from separation to the trailing edge, then rises gradually to the recompression region at the end of the near wake.

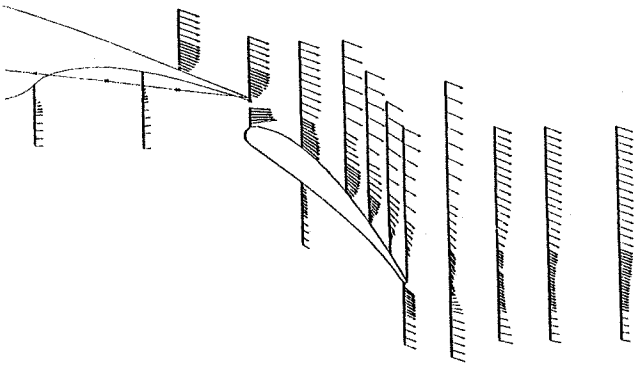

Figure 5. Experimental Velocity Profiles. $\alpha = 7.7°$, $\delta_f = 40°$, Optimum Gap.

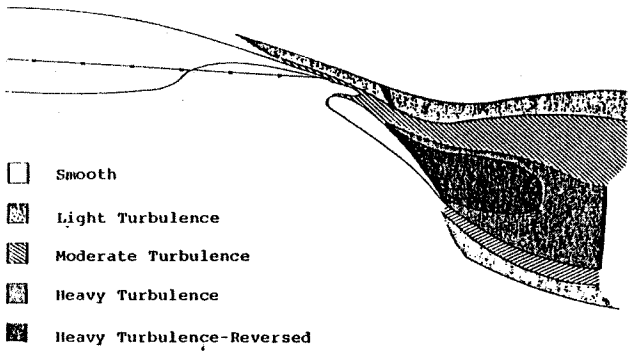

Figure 6. Hot Film Survey. $\alpha = 2.7°$, $\delta_f = 40°$, Optimum Gap.

Flow visualization using oil drops on a longitudinal splitter plate was used by Naik and Pfeiffer (see Ref. 2), revealing the presence of two standing vortices inside the wake, the upper one rotating clockwise for left-to-right flow and the lower one counter-clockwise. The streamline between these two vortices extends from the downstream free stagnation point which defines the end of the wake. The velocity on this streamline has been measured, for various geometries, as 0.2 to 0.35 of the local velocity at the edge of the wake. Inclusion of such sizeable mass and momentum in the analysis seems prudent.

At small angle of attack, α, and large flap angle, δ_f, flow is usually attached on the airfoil and separated on the flap. For large α and small δ_f, the reverse occurs. The presence of a gapped

flap tends to delay stalling of the main airfoil, increasing both maximum lift coefficient and the angle of attack for which it occurs.

III. Potential Flow

For two-dimensional, steady, inviscid, irrotational and incompressible fluid flow in a domain D, the governing equation for the velocity potential Φ is the Laplace's equation,

$$\Phi_{xx} + \Phi_{zz} = 0 \qquad B \in D. \tag{1}$$

$$u = \frac{\partial \Phi}{\partial x}$$

$$w = \frac{\partial \Phi}{\partial z}$$

The boundary B of the fluid domain D contains the surface of the configuration being analyzed.

The airfoil surface is divided into N segments and the (N+1) corner points of these segments are connected by straight lines to form N panels. By introducing the local coordinates for each of the panels, and assuming piecewise linear vorticity distribution and piecewise constant source distribution, the velocity components (u_i, w_i) at a control point i (mid-point of panel i) in the global coordinate system are obtained. Vortex and source strengths are γ and σ. Local coordinates ξ and η are tangent and normal to the panel, with ξ rotated from x by the angle β.

$$\frac{u_i}{U_\infty} = \cos\alpha + \sum_{j=1}^{N} \frac{\gamma_j}{2\pi} U_{ij}^a + \sum_{j=1}^{N} \frac{\gamma_{j+1}}{2\pi} U_{ij}^b + \sum_{j=1}^{N} \frac{\sigma_j}{2\pi} U_{ij}^s \tag{2a}$$

$$\frac{w_i}{U_\infty} = \sin\alpha + \sum_{j=1}^{N} \frac{\gamma_j}{2\pi} W_{ij}^a + \sum_{j=1}^{N} \frac{\gamma_{j+1}}{2\pi} W_{ij}^b + \sum_{j=1}^{N} \frac{\sigma_j}{2\pi} W_{ij}^s \tag{2b}$$

where,

$$\gamma_j = \frac{\gamma_j}{U_\infty} \quad , \quad \sigma_j = \frac{\sigma_j}{U_\infty}$$

$$U_{ij}^a = P_{ij} \sin\beta_j + Q_{ij} \cos\beta_j$$

$$U_{ij}^b = R_{ij} \sin\beta_j + S_{ij} \cos\beta_j$$

$$W_{ij}^a = -P_{ij} \cos\beta_j + Q_{ij} \sin\beta_j$$

$$W_{ij}^b = -R_{ij} \cos\beta_j + S_{ij} \sin\beta_j$$

$$U_{ij}^s = X_{ij} \sin\beta_j + Y_{ij} \cos\beta_j$$

$$W_{ij}^s = -X_{ij} \cos\beta_j + Y_{ij} \sin\beta_j$$

$$P_{ij} = 1 + (1 - \frac{\xi_i}{c_j}) Y_{ij} + \frac{\eta_i}{c_j} X_{ij}$$

$$Q_{ij} = -(1 - \frac{\xi_i}{c_j}) X_{ij} + \frac{\eta_i}{c_j} Y_{ij}$$

$$R_{ij} = -1 + \frac{\xi_i}{c_j} Y_{ij} - \frac{\eta_i}{c_j} X_{ij}$$

$$S_{ij} = -\frac{\eta_i}{c_j} Y_{ij} - \frac{\xi_i}{c_j} X_{ij}$$

$$X_{ij} = -\arctan\left\{\frac{c_j \eta_i}{\xi_i^2 + \eta_i^2 - c_j \xi_i}\right\}$$

$$Y_{ij} = -\frac{1}{2} \ln\left\{\frac{(\xi_i - c_j)^2 + \eta_i^2}{\xi_i^2 + \eta_i^2}\right\}$$

$$\cos\beta_j = \frac{x_{j+1} - x_j}{c_j}$$

$$\sin\beta_j = \frac{z_{j+1} - z_j}{c_j}$$

$$c_j = \left\{(x_{j+1} - x_j)^2 + (z_{j+1} - z_j)^2\right\}^{1/2}$$

$$\begin{bmatrix} \xi_i \\ \eta_i \end{bmatrix} = \begin{bmatrix} \cos\beta_j & \sin\beta_j \\ -\sin\beta_j & \cos\beta_j \end{bmatrix} \begin{bmatrix} x_i^c - x_j \\ z_i^c - x_j \end{bmatrix}$$

$$x_i^c = (x_i + x_{i+1}) / 2$$

$$z_i^c = (z_i + z_{i+1}) / 2$$

The velocity components at a control point i, tangential and normal to the i^{th} panel (u_i^t, u_i^n), are obtained from the velocity components at the control point i in the global coordinate system (u_i, w_i):

$$\begin{bmatrix} u_i^t \\ u_i^n \end{bmatrix} = \begin{bmatrix} \cos\beta_i & \sin\beta_i \\ -\sin\beta_i & \cos\beta_i \end{bmatrix} \begin{bmatrix} u_i \\ w_i \end{bmatrix}_{,i=1,2,..N} \tag{3a}$$

(3b)

Attached Flow

Consider the equation (3b). On the airfoil the normal velocity is equal to zero. Hence the attached flow boundary condition is given by,

$$\text{B.C.:} \qquad u_i^n = 0 \tag{4}$$

with the boundary condition (4), equation (3b) represents a system of N equations in 2N+1 unknowns (N+1 unknown γ's and N unknown σ's). Two unknowns are eliminated by introducing Kutta condition in the following form:

$$\text{Kutta condition: } \gamma_{N+1} = \gamma_1 = 0 \qquad (5)$$

Case 1: Uniformly constant source on the body [4] as shown in Figure 7a.

$$\sigma = \sigma_j, \quad j=1,2,\ldots,N \qquad (6)$$

With (4), (5), and (6), equation (3b) represents a system of N equations in N unknowns and the unknowns can be uniquely determined.

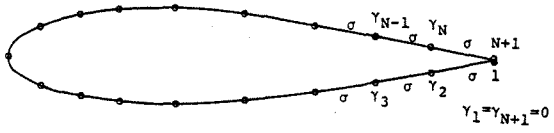

a. UNIFORMLY CONSTANT SOURCE

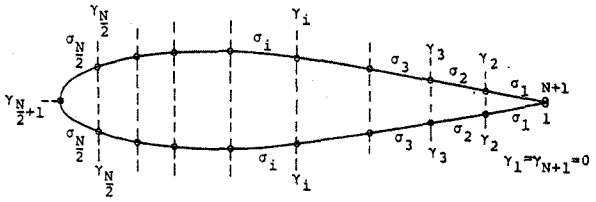

b. PIECEWISE CONSTANT SOURCE

Figure 7. Notation for Panel Modeling for Attached Flow.

Case 2: Piecewise constant sources on the body; Figure 7b.

For this method [8],[9],[10] the airfoil surface is divided into an even number of panels, such that the upper and lower surfaces of the airfoil have equal numbers of panels. The chordwise length of a given lower surface panel is equal to the chordwise length of the corresponding upper surface panel above it as shown in Figure 7b. In this case the piecewise linear vorticity distribution, defined at the panel edges, is retained as in Case 1. But the source distribution is taken to be piecewise constant, defined at the panel mid-points. To reduce the number of unknowns to be the same as that of the equations, the source and vortex density on opposite panels on the upper and lower surfaces are prescribed to be equal. The equal upper and lower formulation for the two-dimensional flows tend to minimize the source gradients and consequently reduce the leakage errors of the constant source panels. This leads to the utilization of fewer number of panels with reasonable accuracy and hence reasonable computing cost.

$$\gamma_{j+1} = \gamma_{N+1-j}, \quad j=1,2,\ldots,\frac{N}{2}-1$$

$$\gamma_{N/2+1} = \gamma_{N/2+1} \qquad (7)$$

$$\sigma_j = \sigma_{N+1-j}, \quad j=1,2,\ldots,\frac{N}{2}$$

With (4), (5), and (7), equation (3b) again represents a system of N equations in N unknowns and the unknowns can be uniquely determined.

Separated Flow

In the separated flow model, vortex distribution alone is prescribed. For the fixed surface panels ($1 \le j \le N$), the distribution of vortex strength is assumed to be linear. For the wake free surface panels ($N \le j \le N2$), the vortex distribution is assumed to be piecewise constant, defined at the panel mid-points as shown in Figure 8. Kutta condition for the separated flow model is introduced in the following form:

$$\text{Kutta Condition: } \gamma_1 + \gamma_{N+1} = 0 \qquad (8)$$

In the equations for the tangential and normal velocity components (3a and 3b), the source term is dropped and the Kutta condition (8) is introduced. These equations must satisfy the following boundary conditions in the appropriate region.

Mixed Boundary Condition

(i) For a control point i on the fixed surface the normal velocity

$$\frac{u_i^n}{U_\infty} = 0, \quad 1 \le i \le N+1$$

(ii) For a control point i on the free surface between N+1 and NF, the surface velocity at the control point is equal to the vortex strength at N+1. Assuming zero internal flow,

$$\frac{u_i^t}{U_\infty} = -\gamma_1; \quad N+1 \le i \le NF \text{ (since } \gamma_{N+1} = -\gamma_1)$$

(iii) Now consider the free surface between NF and N1. The surface velocity at NF is given by

$$\frac{u_{NF}^t}{U_\infty} = -\gamma_1.$$

The surface velocity at N1 is given by

$$\frac{u_{N1}^t}{U_\infty} = V_{N1},$$

where V_{N1} is calculated from the recombination pressure at N1, i.e.,

$$V_{N1} = \sqrt{1 - C_{p\,recomb}}.$$

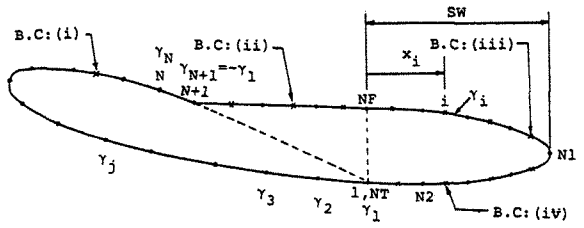

Figure 8. Notation for Panel Modeling for Separated Flow.

The recombination pressure in turn is given by the wake inner flow solution. It is assumed that the velocity from the trailing edge plane to the recombination point decreases by the second power of the ratio of the distance from the trailing edge to the downstream control point under consideration to the distance from the trailing edge to the recombination point, i.e., by the ratio $R(i) = (x_i/SW)^2$ (see Figure 8).

$$\frac{u_i^t}{U_\infty} = -\gamma_1[1 - R(i)] + V_{N1}R(i), \quad NF \le i \le N1$$

(iv) Similarly, for the free surface between N1 and NT, the surface velocity is given by

$$\frac{u_i^t}{U_\infty} = \gamma_1[1 - R(i)] - V_{N1}R(i), \quad N1 \le i \le NT$$

The normal velocity components at the control points on the fixed surface must satisfy the boundary condition (i). The tangential velocity components at the wake free surface must satisfy the boundary conditions (ii), (iii), and (iv) in the appropriate region shown in Figure 8. With the mixed boundary conditions, equations (3a) and (3b) consist of N2 equations in N2 unknown γ's and can be uniquely determined.

For both attached flow and separated flow the velocity components in the global coordinate system are calculated from equations (2a) and (2b). The pressure coefficient at the control points are calculated by means of the formula,

$$c_{p_i} = 1 - \frac{U_i^2}{U_\infty^2}$$

where,

$$U_i^2 = u_i^2 + w_i^2$$

IV. Flow Model

The flow model is solved by matching solutions for outer and inner regions. The outer solution describes the flow past two closed bodies formed by adding to the airfoil and flap:

(a) the boundary layer displacement thickness and
(b) the closed wake behind the airfoil or flap (Fig. 9). The inner solution computes the flow for the interior of the wake. These are solved iteratively until they are compatible at their intersecting surface in shape and pressure.

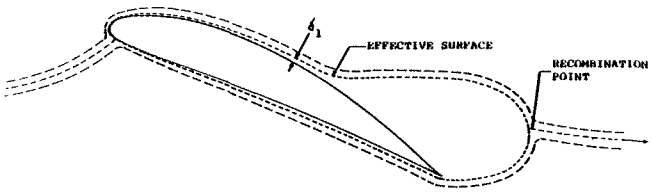

Figure 9. Augmented Airfoil Shape (Outer Flow Model).

Outer Solution

The outer solution uses the potential flow routine described above. Boundary layer displacement thickness is computed and added to the original body with a weighting factor to improve convergence. The augmented airfoil and flap are used in the potential solution to produce new surface pressure and velocity. The boundary layer and potential solutions are iterated until the pressure variation at all points is within specified tolerance.

The boundary layer thickness calculation proceeds from the stagnation point for both the upper and lower surfaces of the airfoil and flap. From the stagnation point to the lower and upper transition points, Thwaites' laminar boundary layer method[11] is used. From transition points to the lower and upper trailing edges, the turbulent boundary layer thickness is calculated by Head's entrainment method.[12] The transition point is located during each iteration, but, until the pressure distribution has converged, separation is prevented by constraining the shape factor. After the pressure values have settled, another turbulent boundary layer calculation is made on the upper surface from transition to trailing edge, using Head's improved entrainment method[13] to locate the separation point.

After the separation point has been found on the upper surface of the augmented airfoil or flap, a wake shape is generated by the potential program and this is iterated until a steady boundary layer solution is obtained which is compatible with the potential flow around a body of a shape similar to that shown in Figure 9.

Inner Solution

The inner solution models and computes the flow inside the closed wake bubble in order to provide a revised value of the pressure at the wake recombination point. This value will then be used in the outer flow calculations in the next iteration.

The flow within the wake is described by defining a few streamlines and by obtaining the

velocity profile at the trailing edge plane. These are shown in Figure 10. Streamlines S and S" define the outer edges of the wake flow. Streamlines S and S' are streamlines issuing from the separation points of the upper and lower surfaces; S" has a velocity equal to that of S and is used as the lower boundary of the wake for the momentum conservation control volume. R and R' are the recombining streamlines which stagnate at a common point near the rear of the wake bubble. The RR' streamline originates at the rear stagnation point and extends both upstream and downstream. Streamline m is the "middle" velocity line, having a velocity which is the average of the local free stream velocity, U_e, and the maximum back flow velocity, U_B. Two trapped, standing vortices are thus identified, the upper bounded by the R and RR' streamlines and the lower by the S' streamline.

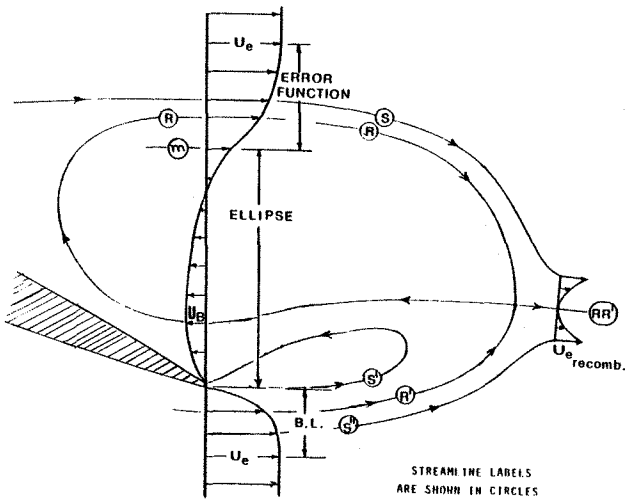

Figure 10. Inner Flow Model.

At the trailing edge plane, the velocities at the upper and lower edges of the viscous wake are equal, since pressure is constant from the separation point to the trailing edge plane.

The upper flow is treated as constant pressure, turbulent, plane jet mixing. Korst's error function velocity profile[14] applies here, except that the sum of velocities U_e and U_B must be used as the driving velocity rather than U_e alone. The origin of the free jet mixing is the point of separation of the boundary layer. The jet profile quickly approaches the fully developed error function profile just as though it had originated at a point further upstream with no boundary layer. This fictitious point, called the virtual origin of mixing, would produce the same mass and momentum deficit as the actual boundary layer. Hill[15] developed equations for this and they have been adapted for two-stream, reversed flow mixing.

For a single stream mixing with a quiescent fluid, Korst gives

$$\frac{U}{U_e} = \frac{1}{2}\left[1 + \text{erf}(\sigma\frac{y}{x})\right] ,$$

where y is the perpendicular distance from streamline m, x is the distance along m from the origin of the mixing, and σ is the jet mixing parameter whose value is well established experimentally to be 12 for incompressible flows.

For two-stream mixing of two semi-infinite parallel and opposite flows (U_e forward and U_B reverse), the above terms must be changed to become

$$\frac{U}{U_e} = \frac{1}{2}\left[\left(1 - \frac{U_B}{U_e}\right) + \left(1 + \frac{U_B}{U_e}\right)\text{erf}\left(\sigma\frac{y}{x}\right)\right] \quad \text{and}$$

$$\sigma = 12\left[\frac{U_e - U_B}{U_e + U_B}\right]$$

However, in the wake, U_B is not the velocity of a uniform semi-infinite flow, but is the maximum velocity between two non-potential vortices. Thus, the above equations are accepted for the upper half of the mixing region but the lower portion (inside m) is better modeled by a portion of an ellipse which matches the velocity at streamline m, is zero at the trailing edge, and has U_B as its maximum upstream velocity. Below the airfoil, the flow velocity is described by the turbulent boundary profile produced by the outer flow solution.

At the trailing edge, mass conservation equations are written:

(1) Mass flows between S and an arbitrary edge streamline e are equal at separation and at the trailing edge plane.

(2) Net mass flow between S and the airfoil surface is zero.

(3) Mass flows are equal between S and R and between S' and R'.

A control volume formed by the trailing edge plane, streamlines S and S", and the small outflow area shown in Figure 8 is used for momentum conservation in the chordwise direction. For this, pressures on the S and S" streamlines supplied by the outer solution are summed. The empirical function of Nash[16] relates to the total pressure of streamlines R and R' to the obtainable recompression pressure. The three mass and one momentum equations are solved simultaneously for streamlines m, S and R and the back flow velocity U_B. The empirical Nash factor provides a revised value of pressure at the recombination point at the end of the wake.

Final Convergence

The new recombination pressure is taken back to the potential solution. Iteration between outer and inner solutions continue until the pressure values converge. In practice, the inner solution is never called more than three times before convergence is achieved. A final potential flow computation is made to smooth the wake, then forces and moments are calculated by integrating the pressures on the body surface. A schematic flow chart is shown in Figure 11.

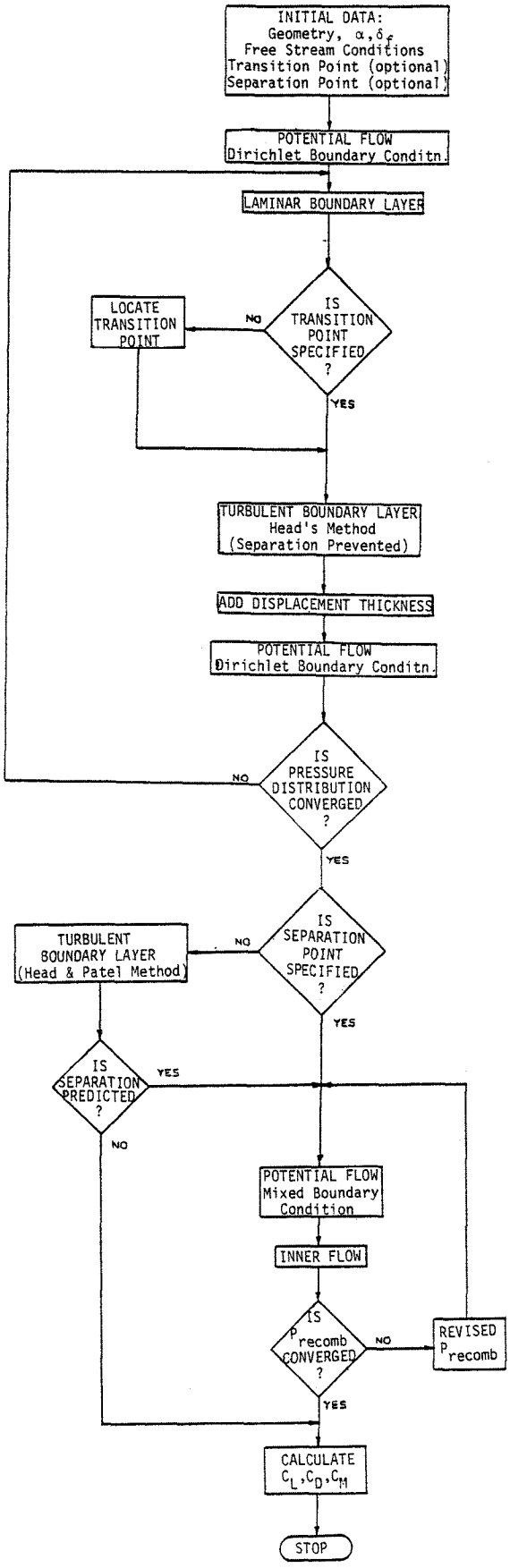

Figure 11. Computational Flow Model.

In addition to the input data listed in the top "box" of Figure 11, the following quantities are generated internally by the program as initial, trial values: pressure at the recombination point, trial wake shape, and back flow velocity.

V. Computed Results

Computations were first made to test the accuracy of the potential program alone. Attached flow around a two-element airfoil was calculated and found to agree almost exactly with the exact conformal transformation solution.

Single Element Airfoil

Next, computations of attached and separated flow on a single-element GA(W)-2 airfoil were made and compared with experimental data.[17][18] Computer runs were for angles of attack of 0, 8, 10, 14, 16, and 18 degrees. Predicted separation points agreed well with experimental ones until $\alpha = 18°$, where the separation occurred at 25° chord. When the experimental separation location was specified, the pressure distribution matched the data well, as was true for the lower angles of attack. Lift and pitch moment results are shown in Figure 12. It can be seen that maximum lift coefficient was predicted accurately.

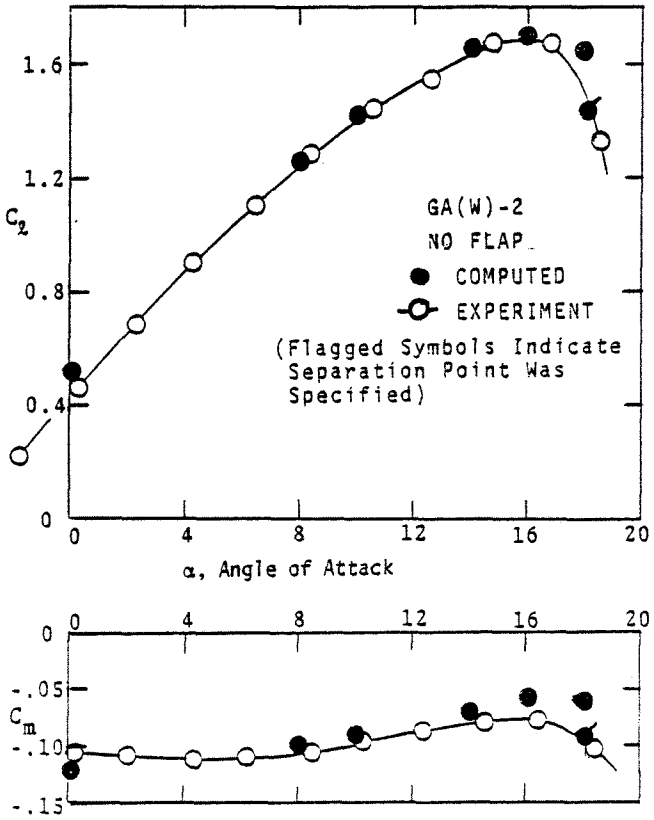

Figure 12. Comparison of Lift and Pitch Moments for a Single-Element Airfoil.

The integral method of boundary layer calculation appears to be inadequate for accurately predicting separation on the front half of the

airfoil where pressure gradients are quite large. Other boundary layer methods will be tried to improve the calculations in the post-stall regime.

Airfoil with Flap

Separated flow on a GA(W)-1 airfoil with a 30% flap was then computed and compared with data from Refs. 19 and 20. Computer runs were made generally to match the experimental angles of attack: 0.2, 2.7, 5.2, 7.7, 10.3, and 12.8 degrees with 40° flap deflection; 0.1, 5.2, 10.3, 12.8, and 15.5 degrees with 30° flap deflection. Typical pressure distribution results are shown in Figures 13 and 14. The experimental C_p values have not been corrected for wind tunnel wall effects.

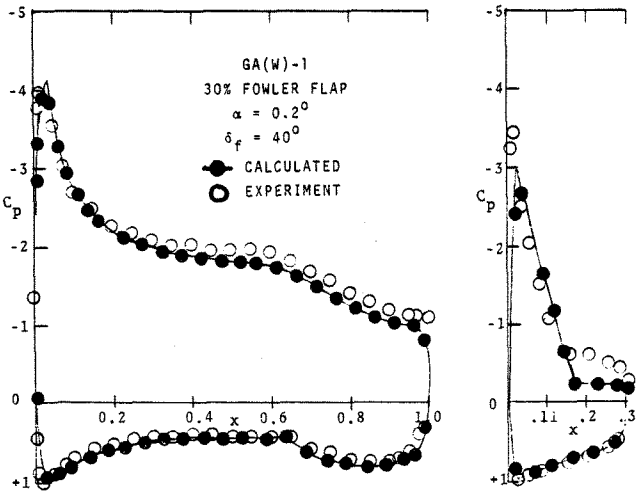

Figure 13. Comparison of Pressure Distributions for an Airfoil-with-Flap.

In the pre-stall region ($\alpha<10°$), experiment and calculation both show attached flow on the airfoil and separated flow on the flap. In the post-stall region ($\alpha>12°$), both predicted separation on the airfoil and attached flow on the flap (although prediction of the separation location was not accurately obtained). The exchange of separation occurrence from flap to airfoil appears to take place just after maximum lift angle and may be considered to be the stall criteria for this airfoil. It would be instructive to see whether this is true for flapped airfoils in general. For this airfoil, no combination of angle of attack and flap angle was found either by computation or experiment where both elements had large separated flow regions. For highly separated flap, airfoil separated at about 90% in both computer and wind tunnel.

Further evidence that the separation switches elements at stall is given by the one computation that did not predict the correct element to be separated. At α = 10.3° and δ_f = 40° the computer program predicted separation on the flap while experiment showed that it had shifted to the airfoil.

Comparisons of computed results with experiment are shown in Figure 15 for lift, Figures 16 and 17 for pitch moment, and Figures 18 and 19 for drag. The experimental data have been corrected for wind tunnel boundary effects. For the computed drag values, no skin friction corrections have been added; attempts to make simple Squire-Young skin friction estimates were found to be inaccurate.

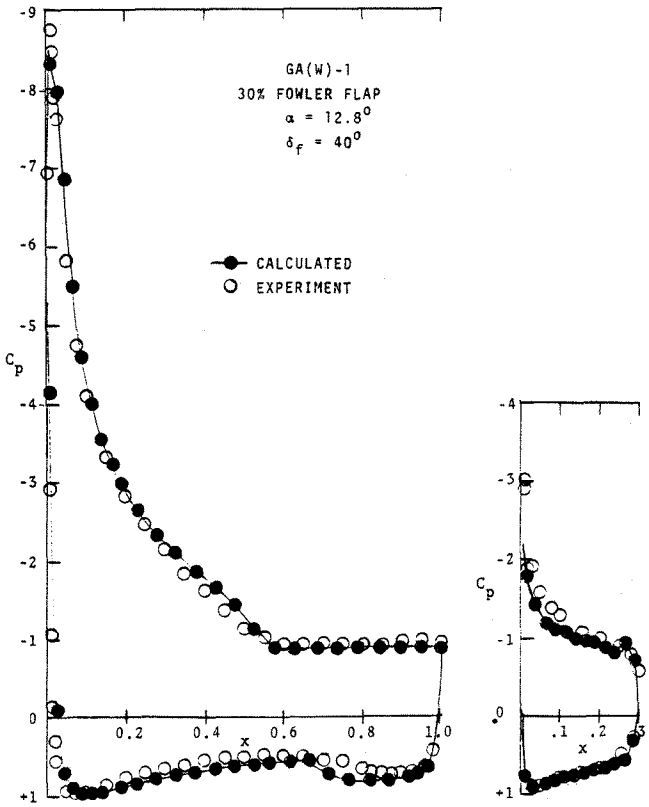

Figure 14. Comparison of Pressure Distributions for an Airfoil-with-Flap.

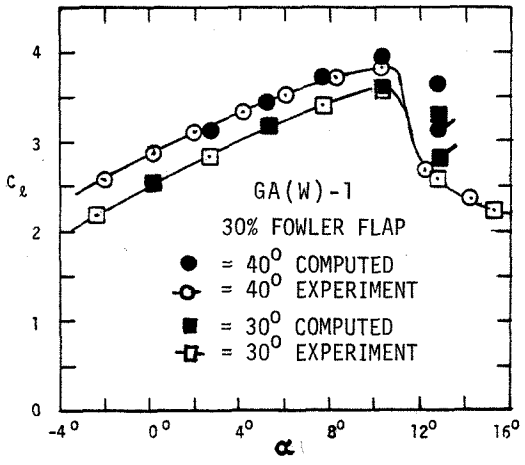

Figure 15. Comparison of Lift for an Airfoil-with-Flap.

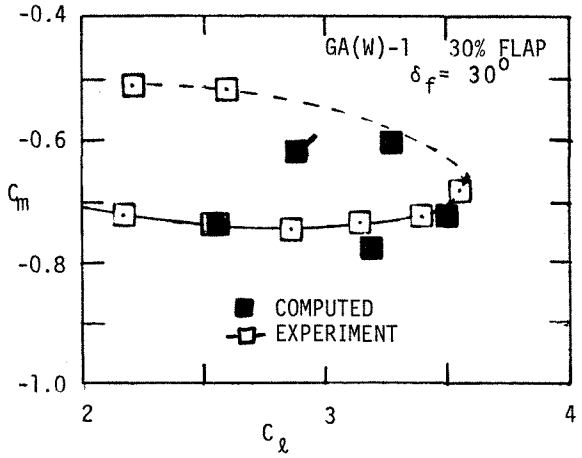

Figure 16. Comparison of Pitching Moment for an Airfoil-with-Flap.

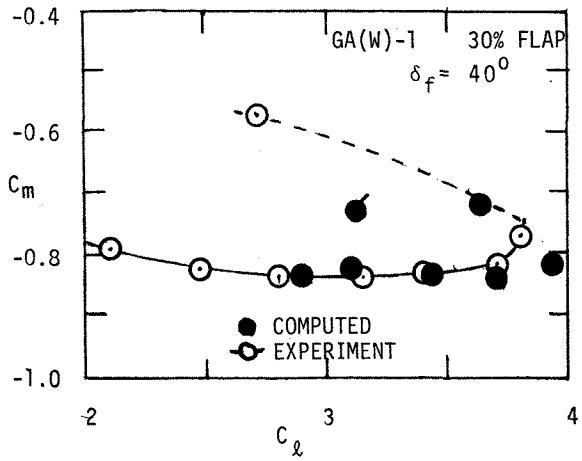

Figure 17. Comparison of Pitching Moment for an Airfoil-with-Flap.

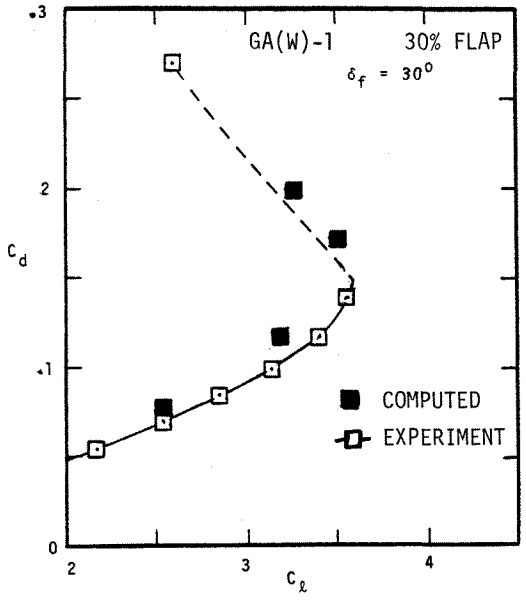

Figure 18. Comparison of Drag for an Airfoil-with-Flap.

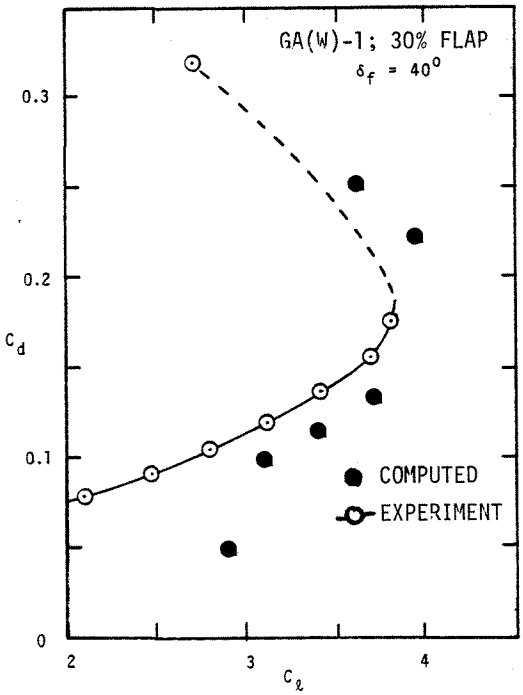

Figure 19. Comparison of Drag for an Airfoil-with-Flap.

Limitations

The current computer code is limited to incompressible flow, a restriction which can be removed with a reasonable effort. It does not permit laminar separation, either of the short or long bubble types. Only two elements have been computed, but the potential program has been written in general form so that more elements can be treated. Multiple flaps could create difficulties in wake modeling, but none are foreseen.

Computing Time

All computations were performed on an IBM 370 Computer, Model 3031. CPU time (interactive mode) was 2 to 2.5 minutes per run with a cost of about $15.

VI. Conclusions

A flow model and computer program have been developed for an airfoil with a gapped-flap which (a) includes the physically significant separated-flow features, (b) requires no a priori knowledge of separation location or pressure or wake shape, (c) requires a very modest amount of computation time, and (d) has produced accurate results for the airfoils computed.

VII. References

1. Zumwalt, G.W., and Naik, S.N.: "An Analytical Method for Highly Separated Flow on Airfoils at Low Speeds," NASA-CR-145249, May 1977.

2. Pfeiffer, N.J., and Zumwalt, G.W.: "Computational Model for Low Speed Flows Past Airfoils with Spoilers," AIAA J., Vol. 20, No. 3, pp. 376-382, March 1982.

3. Zumwalt, G.W., and Carlson, R.J.: "A Computational Model for Incompressible Flow Past an Airfoil with a Highly Deflected Aileron," AIAA Paper No. 82-0019, January 1982.

4. Maskew, B.: INVERSE Program marketed by Analytical Methods, Inc., Bellevue, Washington, 1979.

5. Elangovan, R.: "Analysis of Incompressible Separated Flow Around an Airfoil with a Finite-Gap Flap," Ph.D. Dissertation, Wichita State University, May 1982.

6. Elangovan, R., and Zumwalt, G.W.: "Analytical Model and Computer Program for Flow Past Airfoils with Finite-Gap Flaps," Aero. Rept. 82-3, Wichita State University, Wichita, KS, June 1982.

7. Seetharam, H.C., and Wentz, W.H., Jr.: "A Low Speed Two-Dimensional Study of Flow Separation on the GA(W)-1 Airfoil with 30-Percent Chord Fowler Flap," NASA CR-2844 (1977).

8. Maskew, B., Woodward, F.: "Symmetrical Singularity Model for Lifting Potential Flow Analysis," Journal of Aircraft, Vol. 9, pp. 733-734, September 1976.

9. Bristow, R.: "Improvements in Surface Singularity Analysis and Design Methods," NASA CR-2045, pp. 221-236, March 1978.

10. Papadakis, M.: "Computer Analysis of Wing Design for General Aviation Aircraft," Loughborough University Master of Science Thesis, 1981.

11. Thwaites, B.: "Approximate Calculation of the Laminar Boundary Layer," Aero. Quart., Vol. 1, p. 245, 1949.

12. Head, M.R.: "Entrainment in the Turbulent Boundary Layers," ARC R&M 3152, 1958.

13. Head, M.R., and Patel, V.C.: "Improved Entrainment Method for Calculating Turbulent Boundary-Layer Development," ARC R&M 3643, 1969.

14. Korst, H.H.: "A Theory for Base Pressures in Transonic and Supersonic Flow," J. App. Mech., Vol. 23, No. 4, p. 593, December 1956.

15. Hill, W.G., Jr., and Page, R.H.: "Initial Development of Turbulent, Compressible Free Shear Layers," J. Basic Engineering, Vol. 91, Series D, No. 1, March 1969, pp. 67-73.

16. Nash, J.F.: "An Analysis of Two-Dimensional Turbulent Base Flow, Including the Effects of the Approaching Boundary Layers," ARC R&M 3344, July 1962.

17. Wentz, W.H., Jr., and Fiscko, K.A.: "Pressure Distributions for the GA(W)-2 Airfoil with 20% Aileron, 25% Slotted Flap and 30% Fowler Flap," NASA CR-2948, 1978.

18. Seetharam, H.C., Rodgers, E.J., and Wentz, W.H., Jr.: "Experimental Studies of Flow Separation of the GA(W)-2 Airfoil at Low Speeds," AR 77-4, Wichita State University, Wichita, KS, 1977.

19. Wentz, W.H., Jr., Seetharam, H.C., and Fiscko, K.A.: "Force and Pressure Tests of the GA(W)-1 Airfoil with a 20% Aileron and Pressure Tests with a 30% Fowler Flap," NASA CR-2833, 1977.

20. Wentz, W.H., Jr., and Seetharam, H.C.: "Development of a Fowler Flap System for a High Performance General Aviation Airfoil," NASA CR-2443, 1974.